JOURNAL OF APPLIED ELECTROCHEMISTRY 24 (1994) 652–657

A photophysical technique for the measurement of local oxygen concentration near an electrode surface

V. LESCURAS, I. ZOUARI, G. VALENTIN, F. LAPICQUE

Laboratoire des Sciences du Génie Chimique, CNRS-ENSIC-INPL, BP 451, F-54001 Nancy, France

J. C. ANDRÉ

Département de Chimie Physique des Réactions, CNRS-ENSIC-INPL, BP 451, F-54001 Nancy, France

Received 10 May 1993; revised 11 November 1993

Electrochemical processes involving gas production are of great technical importance but the mechanisms involved in the growth of electrogenerated bubbles and transport processes involving gas near an electrode still remain obscure. This paper describes an original technique, based on the inhibition of the fluorescence of an appropriate substance by dissolved oxygen, for the measurement of the *local* concentration of dissolved oxygen near an electrode. The possibilities offered by this technique and typical results are presented and discussed.

1. Introduction

Electrogenerated gas is produced by a sequence of several steps. First, an electrolytic process occurs involving dissolved matter, which is followed by bubble nucleation and then growth. Gas supersaturation is to be expected near the electrode surface at low rates of nucleation or growth, and may be an alternative method for supplying concentrated dissolved gas in reactors, e.g. oxygen in chemical or biochemical reactors [1]. In addition, the phenomenon of supersaturation is of obvious fundamental interest. An analogy between electrolytic bubbles and vapour formation in boiling liquids has already been developed by several authors. In particular, several attempts have been made to establish models for bubble growth [2] and mass transfer at gas–liquid interfaces [3]. The various models described in the literature show the complexity of this phenomenon [2, 3].

The supersaturation of electrogenerated gas has been investigated over the last thirty years by using microelectrodes or transient electrochemical techniques. For the case of hydrogen evolution on a platinum surface, measurements of overpotential and the observation of the potential transient indicates concentrations up to five times the saturation value [4, 5]. More recently, Bon and Tobias [6] obtained concentrations at an electrode corresponding to a hydrogen pressure of between 4 and 70 bars, depending on the operating conditions. Oxygen evolution was later investigated by Shibata [7] using a galvanostatic method which showed concentrations 70 times greater than the saturation value. Other devices e.g. the rotating disc cone electrode, have been used for investigating the evolution of hydrogen [8] or the production of oxygen [9]. Pressures corresponding to between 10 and 36 bars were reported. Theoretical studies based on Scriven's model [10] and taking into account the growth rate of oxygen bubbles, showed that the concentration could attain 36 times its saturation value [10, 11].

All the methods mentioned above yield estimates for the concentration of dissolved matter at the electrode surface. However, the spatial distribution of this concentration is not directly available. Concentration profiles can be obtained by a theoretical model of oxygen transport from the electrode surface to the bulk, in relation to its transfer to an existing bubble. Nefedov *et al.* [12] recently measured oxygen concentration profiles using either a microdisc facing the gas evolving electrode, or a high speed photography. Supersaturation was claimed to exist only in a 50 μm thick layer near the electrode surface [12].

This paper presents a new method for determining the local concentration of dissolved oxygen, based on fluorescence inhibition. A laser beam is focused near a small platinum electrode which is the source of oxygen production in a solution containing a fluorescent substance. The fluorescence emitted by the focal zone, with reference to that where oxygen is absent, gives the local oxygen concentration. Concentration profiles of oxygen near the electrode surface are obtained and discussed.

2. Fluorescence inhibition by oxygen

Substances which fluoresce are excited by absorption of radiation of a suitable wavelength. The back transition to the fundamental state is accompanied by light emission at a longer wavelength. Fluorescence is the light emitted in a singlet–singlet transition to the fundamental state. Oxygen can quench fluorescent emission by absorbing the energy of the excited

This paper was presented at the International Workshop on Electrodiffusion Diagnostics of Flows held in Dourdan, France, May 1993.

0021-891X 1994 Chapman & Hall

molecule. This side phenomenon hinders fluorescence and is the principle of the method used here for measuring the local concentration of dissolved oxygen.

The following photonic processes are involved:

$$M + h\nu_e \longrightarrow M^*$$

Absorption of the excitation light at a rate I_a

$$M^* \longrightarrow M + h\nu_f$$

Fluorescence emission with rate constant k_f

$$M^* + O_2 \longrightarrow M + O_2^*$$

Inhibition by oxygen with rate constant k_i

$$M^* \longrightarrow M$$

Nonradiative transition, with rate constant k_n

All the processes can be assumed to be first order with respect to all species. Therefore, the rate of formation of excited M^* may be expressed as

$$\frac{dM^*}{dt} = I_a - k_f(M^*) - k_i(M^*)(O_2) - k_n(M^*) \quad (1)$$

Assuming steady-state conditions, the formation rate is equal to zero and

$$I_a = (M^*)[k_f + k_n + k_i(O_2)] \quad (2)$$

The fluorescence intensity is defined as the product $k_f(M^*)$ and can be written as

$$I_f = \frac{I_a k_f}{[k_f + k_n + k_i(O_2)]} \quad (3)$$

In the absence of oxygen, fluorescence is emitted with an intensity I_{fo} given by

$$I_{fo} = \frac{I_a k_f}{[k_f + k_n]} \quad (4)$$

Combining the above two expressions for fluorescence intensity leads to the Stern–Volmer relation:

$$\frac{I_{fo}}{I_f} = 1 + \frac{k_i(O_2)}{k_f + k_n} \quad (5)$$

This equation states that the oxygen concentration can be determined by measurement of the fluorescence intensity in an oxygen-free solution, and in actual conditions of oxygen production.

Using suitable optical devices, and provided there is a sufficient convergence of the beam, a laser can be focused to a point of less than 30 μm diameter. Thus, without perturbing the electrochemical reaction, this technique allows the measurement of local oxygen concentrations by the fluorescence emitted from such small focal zone.

3. Molecule and laser

Pyrene tetrasulfonic acid (PTSA) was selected for this study since this molecule exhibits significant fluorescence inhibition by oxygen over a suitable range of pressure [13] and is of sufficient solubility in water or in aqueous solutions. In addition, this molecule has very different wavelengths for absorption and fluorescence emission. One absorption peak is in the range 290–330 nm and a continuous He–Cd laser ($\lambda = 325$ nm) was therefore used. Significant fluorescence intensity at 405 nm was measured for PTSA concentrations near 10^{-5} M in a 0.1 M NaOH solution.

3.1. *Electrical stability of the molecule*

The stability of PTSA in an electrical field was initially verified at the bench scale. Oxygen was generated at a platinum coated titanium electrode (area $\approx 40\,cm^2$) for a period of 10 min at controlled potential with continuous recording of the electrical current. The electrolyte solution was 10^{-5} M PTSA in a 0.1 M NaOH medium. Both absorption and fluorescence spectra were compared before and after electrolysis. Appreciable changes in the spectra were observed when the electrode potential exceeded 1.30 V vs SCE for more than two hours. The average corresponding current density was close to $100\,A\,m^{-2}$. Additional experiments showed that the molecule had an acceptable stability at current densities of up to $1000\,A\,m^{-2}$, but for shorter periods.

3.2. *Calibration*

Fluorescence inhibition was calibrated in a glass cell operating at gas pressures up to 10 bars, as shown in Fig. 1. The volume of the cell was approximately $20\,cm^3$. For this purpose, the fluorescence signal was measured in an equilibrium solution having a gas phase of known oxygen partial pressure. Varying this pressure from 0 to 5 bars gave a calibration plot. Because of the slow rate of gas–liquid mass transfer, the cell was thoroughly shaken several times between short rest periods. Equilibrium was assumed to be attained when the fluorescence signal from the solution became steady. The oxygen pressure was measured at an equilibrium using a manometer with an accuracy of 0.05 bars. Fluorescence emitted in an oxygen-free solution was observed by reducing the gas pressure in the glass cell down to 10^{-3} atm, using a vacuum pump for approximately 30 min. The intensity of the fluorescence signal U, obtained for various partial pressures of oxygen,

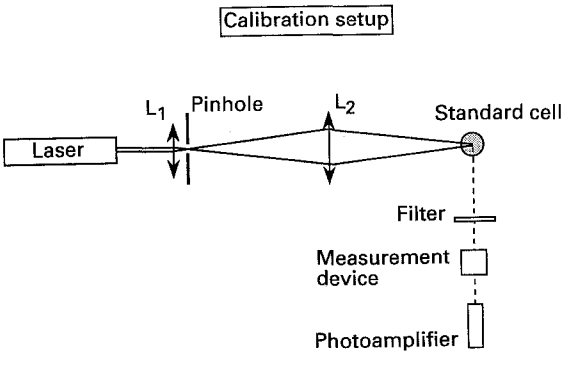

Fig. 1. Experimental setup for calibration of the fluorescence technique.

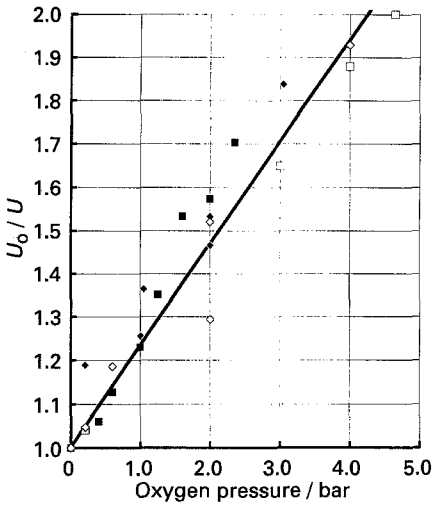

Fig. 2. Calibration curve of fluorescence inhibition by dissolved oxygen, expressed in the form of a Stern–Volmer relationship: U denotes the signal delivered by the photoamplifier at oxygen pressure $P(O_2)$.

was plotted using the Stern–Volmer relation. Because of its importance in estimating the oxygen concentration, or its corresponding partial pressure, calibration was repeated four times and experimental data were found to be of a satisfactory consistency (Fig. 2). The following relation was obtained:

$$\frac{U_0}{U} = 1 + 0.235 P_{O_2} \qquad (6)$$

where P_{O_2} is the oxygen partial pressure (bars) in equilibrium with the 10^{-5} M PTSA, 0.1 M NaOH solution and U_0 is the fluorescence signal measured in an oxygen-free solution.

The amount of dissolved oxygen in the electrolytic cell was expressed in terms of the corresponding pressure P_{O_2} in equilibrium with the alkaline solution. The fluorescence signal at $P_{O_2} = 0$ could not be measured in this cell and was therefore estimated from the intensity observed under ambient conditions, with no oxygen evolution (i.e. for $P_{O_2} = 0.21$ bar), using the calibration relation (Equation 6).

4. Experimental device

Figure 3 shows a schematic diagram of the experimental setup. The optical components were fixed on an optical bench and the electrolytic cell was attached to a X-Y-Z microcontroller table.

4.1. *Optical device*

The optical system was designed to allow accurate focusing of the He–Cd laser beam in a defined volume in the electrolyte solution (Fig. 3). Lenses 1 and 2 broaden the beam and the small numerical aperture avoids the microscope objective getting in the way of the beam. The laser was then focused to a small volume (diameter $\approx 30\,\mu$m) by the large numerical aperture lens 3. This system ensures focusing on an accurately located small volume of liquid. All optical components upstream from the electrolytic cell were

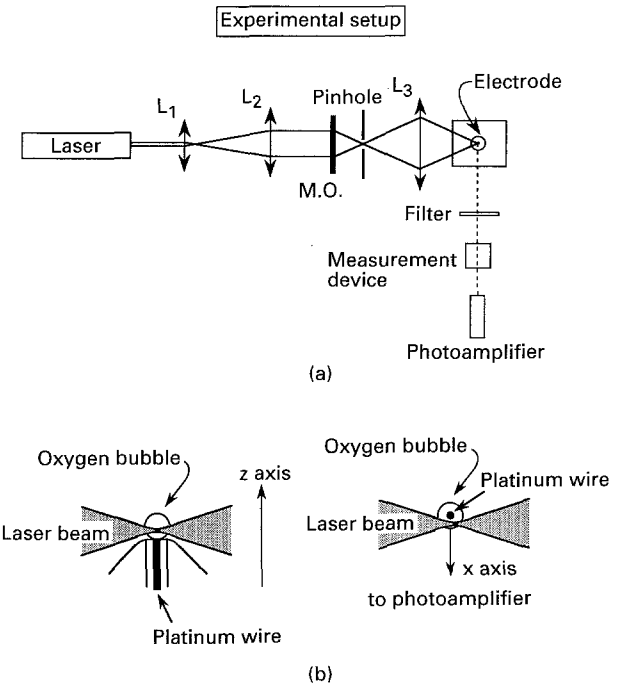

Fig. 3. Measurement of local oxygen concentration in the liquid phase. (a) Experimental setup. (b) Views of the electrode tip and the oxygen bubble: side view on left and top view on right.

purchased from Ealings, France and were compatible with u.v. wavelengths.

When irradiated by a concentrated laser beam the liquid volume emitted high density fluorescence in all directions of space. In order to avoid damaging the amplifier by the incident beam fluorescence was measured perpendicular to the laser beam. Even though the incident beam and the emitted fluorescence are of different wave lengths, and despite the fact that measurements were made at a 90° angle, an interferenciel filter at 405 nm was located between the cell and the photoamplifier to avoid the side-absorption of incident light. Two double lens, (Melles-Griot, France) were installed on the measurement axis focusing the emission from the test volume in to a 80 μm pinhole close to the photoamplifier. The amplifier was mounted on a secondary X-Y-Z microcontroller table and its location was carefully checked by measuring the maximum fluorescence.

4.2. *Electrolytic cell*

Experiments were conducted in stationary fluid in a parallelipipedic cell made from plates of Altuglas™ (methyl polymethacrylate) and provided with quartz windows for the laser beam and the emitted fluorescence. The working electrode was a 100 μm diameter platinum wire, embedded in an Altuglas cylinder (Fig. 4). The conical end of the electrode support was machined and smoothed with emery paper and diamond paste. A sheet of expanded platinum coated titanium acted as the counter-electrode. The electrode potential was referred to a saturated calomel electrode located in the cell. The cell was enclosed in a lightproof box.

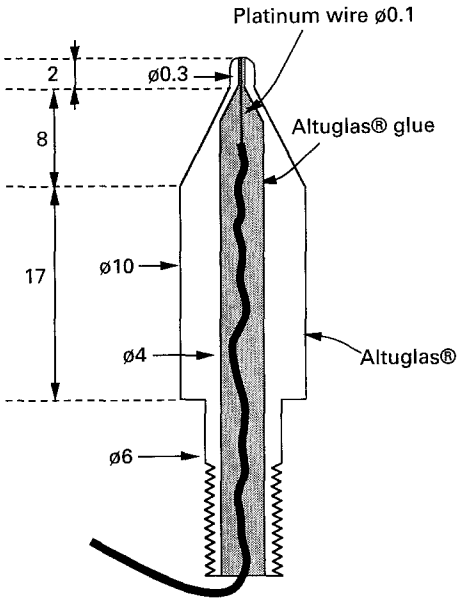

Fig. 4. Schematic view of the platinum electrode; distances are given in millimetres.

4.3. *Experimental procedure*

The platinum electrode was activated by hydrogen evolution at −1.25 V vs SCE for 10 min prior to fluorescence measurements. A positive potential was then applied to the electrode for 5–20 min, depending on the current density for oxygen production. For lower current densities, the cell current was shut off before measurements. For higher current densities, the electrode potential was reduced to 0.7–0.9 V vs SCE to avoid bubble detachment from the electrode surface. However, the first series of measurements was found to give data of poor reliability and was subsequently considered to be only an additional activation of the electrode.

The box surrounding the electrolytic cell prevented continuous observation of the electrode surface and attached bubbles. After a series of fluorescence measurements the bubble diameters were determined by means of a microscope eyepiece to an estimated tolerance of 50 μm.

5. Results

Preliminary experiments showed the feasibility of the online technique in that oxygen production was observed to give an appreciable reduction in fluorescence intensity. Moreover, transient signal peaks indicated bubble detachment from the metal surface and sudden changes in the concentration profile due to the bubble motion. Transient oxygen production and the effects of the interface near the electrode were investigated prior to measurement of the concentration profile.

Bubble diameter was found to increase with current density, in good agreement with the conclusions of Janssen and Hoogland [14]. The diameters of typical oxygen bubbles increased from 150 μm at 50 A m^{-2} to 500 μm at 1200 A m^{-2}. However, the bubble diameter was also influenced by the roughness of both the platinum surface and the edge of the insulator. Thus a 300 μm bubble could be formed at 30 A m^{-2} if there was a rougher surface.

5.1. *Fluorescence decay transient*

Fluorescence decays were measured for oxygen production experiments at controlled potential. The distance z between the electrode surface and the focal point was 50 μm. The current rapidly decreased and, in most cases, reached a constant value after a few minutes. Signal decay exhibited similar variations reaching a steady-state level after 5 min. The corresponding oxygen pressure was in the range of 5–10 bars, depending on operating conditions.

A first attempt at modelling was made by neglecting bubble formation and considering only the electrolytic production of oxygen and its diffusion in the liquid. Solving Fick's law with a constant concentration gradient at the electrode, neglecting the time variation of current density, yielded expressions for the oxygen concentration with time and distance, $C(z, t)$. The theoretical relation was based on the reduced variable $\boldsymbol{C}$

$$\boldsymbol{C} = \frac{C - C_{t=0}}{C^*}$$

where C^* denotes oxygen solubility under atmospheric pressure (1.29 mol m^{-3} at 20° C) and $C_{t=0}$ is the initial concentration. For current densities of 1000 and 100 A m^{-2}, respectively, the reduced concentration at $z = 100$ μm can exceed 20 for 1.5 s and 20 s, respectively (Fig. 5). As shown in Fig. 5, experimental variations are much slower than predicted by the model. The large discrepancy is due to the amount of gas formed and the presence of an interface near the focal point. More realistic models are required for quantitative interpretation of fluorescence decay.

5.2. *Effect of an interface on fluorescence measurement*

The incident laser beam is affected by the presence of a phase discontinuity. A change in refractive index

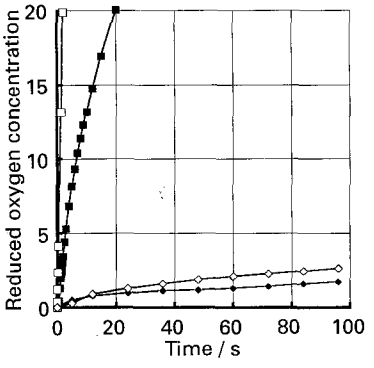

Fig. 5. Time variation of the concentration of dissolved oxygen from the electrode surface. Comparison of experimental results with predictions from the model, neglecting bubble formation. Current densities: (■) 100 (theoretical), (□) 1000 (theoretical), (◆) 700 (experimental) and (◇) 1200 (experimental) A m^{-2}.

results in reflection and diffraction around the object, deviates the laser beam in the gas phase and consequently modifies the excitation in the liquid. In addition, fluorescence emitted by the irradiated zone near an interface may also undergo similar phenomena. Both effects alter the fluorescence measurements and the estimation of local oxygen concentration.

Simulation tests were carried out using objects of comparable size (200–800 μm): (i) hydrogen bubbles and (ii) glass spheres glued to the electrode tip. Fluorescence intensity profiles were measured along the axis of the photoamplifier, i.e. perpendicularly to the incident beam. Coordinate x was arbitrarily considered as positive when the focal point was located between the electrode tip and the photoamplifier. Figure 6 relates to profiles generated by solids and shows the significant effect of the interface, especially when the laser is focused at the bottom of the sphere ($x = 0$). The decrease in the fluorescence signal corresponds to oxygen pressures up to 2 bars. For negative values of x, the sphere partly hides the emitted fluorescence and the signal intensity is underestimated. This corresponds to apparent pressures of 0.5–0.8 bars for x below −0.5 mm. The well-defined and symmetrical peak of the concentration profile is due to the maximum effect of the spherical interface (Fig. 6) and the peak width is of the same order of magnitude as the sphere diameter. The effect becomes negligible as the laser is focused far from the sphere and the oxygen pressure reaches its bulk value (0.21 bar) for $x > 0.5$ mm. It should be noted that the electrode also alters the fluorescence signal and results in an apparent supersaturation (Fig. 6).

The profiles obtained with hydrogen bubbles are shown in Fig. 7. Their behaviour can be seen to be almost the same as for glass spheres and the apparent gas pressure is of the same order, for comparable diameters. The maximum apparent oxygen pressure is obtained for a 800–900 μm diameter hydrogen bubble, and it seems that the larger the bubble, the more significant is this side-phenomenon.

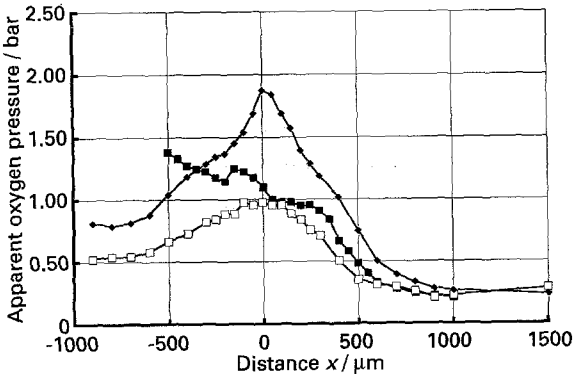

Fig. 6. Effect of a solid phase (electrode tip or glass sphere) on the fluorescence signal. The observed signal was converted into apparent oxygen pressure; x is the coordinate in the direction of the photoamplifier. Key: (■) electrode tip, (□) $\phi = 360$ μm and (◆) $\phi = 570$ μm.

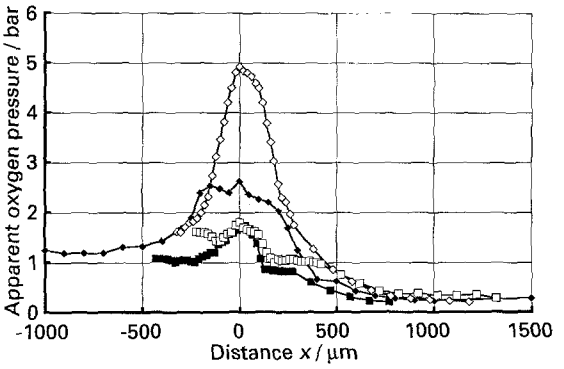

Fig. 7. Effect of a hydrogen bubble on the fluorescence signal. The observed signal was converted into apparent oxygen pressure; x is the coordinate in the direction of the photoamplifier. Bubble diam., ϕ: (■) 200, (□) 250, (◆) 500 and (◇) 850 μm.

5.3. *Concentration profiles of dissolved oxygen*

The concentration profiles were measured under steady-state conditions. The fluorescence signal at a given location was checked at the end of a scan in one direction. The results have a satisfactory consistency indicating that there are only small variations in bubble size and concentration profiles with time. The relative stability of measurements with time is probably due to the small amount of oxygen produced.

Concentration profiles on the axis of the photoamplifier are reported in Figs 8, 9 and 10 for various current densities and for bubbles of the same diameter. For z of about 50 μm, the profiles exhibit a well-defined maximum at $x = 0$, but the observed concentration depends strongly on the bubble diameter. For the smallest bubbles, the observed fluorescence signals for oxygen evolution do not significantly differ from those recorded for hydrogen bubbles (Fig. 8). Increasing the oxygen current density results in higher fluorescence inhibition. The corresponding oxygen pressure at $x = 0$ reaches 2 bars at 100 A m^{-2}, 3 bars at 400 A m^{-2} and 10 bars at 1200 A m^{-2} (Figs 9 and 10). These results are lower than those published for concentrations at the electrode surface. For instance, supersaturation has been reported, ([8]

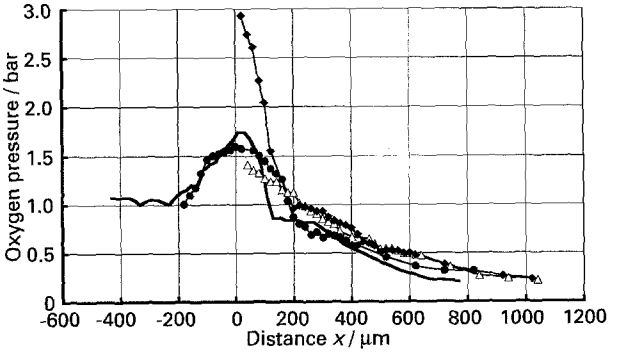

Fig. 8. Profiles of oxygen concentration measured at a vertical distance z of 50 μm from the electrode tip. The bubble diameter was in the range 150–200 μm for all experiments. Symbols refer to oxygen evolution at i and the solid line is the apparent concentration observed with a 200 μm hydrogen bubble. (——) Electrode tip. Current densities: (△) 38, (◆) 65 and (●) 83 A m^{-2}.

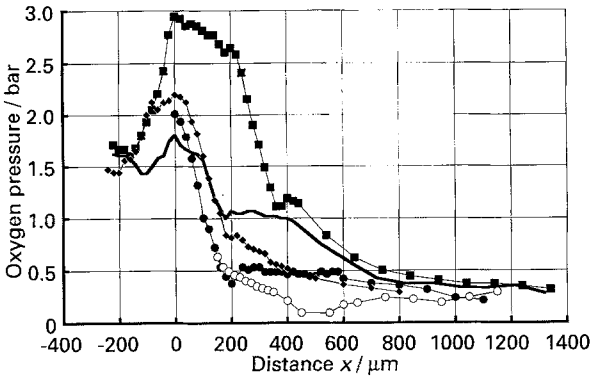

Fig. 9. Profiles of oxygen concentration measured at a vertical distance z of 50 μm from the electrode tip. The bubble diameter was about 300 μm for all experiments. Symbols refer to oxygen evolution at i and solid line (——) is the apparent concentration observed with a 300 μm hydrogen bubble. Current densities: (■) 450, (●) 123, (◆) 97 and (○) 28 A m^{-2}.

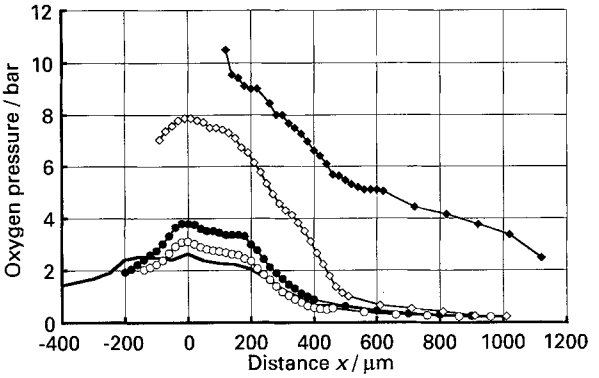

Fig. 10. Profiles of oxygen concentration measured at a vertical distance z of 50 μm from the electrode tip. The bubble diameter was in the range 400–500 μm for all experiments. Symbols refer to oxygen evolution at i and the solid line (——) is the apparent concentration observed with a 500 μm hydrogen bubble. Current densities: (○) 486, (●) 664, (◇) 703 and (◆) 1200 A m^{-2}.

or [7]), to be almost 6 bars at 100 A m^{-2} [8] and 14 or 50 bars at 500 A m^{-2}. The discrepancy is due to the different experimental techniques used in the investigations. In addition, contrary to published data, values presented here are related to supersaturation phenomena at 50 μm from the electrode surface.

The decrease in pressure occurs mainly for x below 400 μm; the corresponding pressure at this location is in the range 0.5–4 bars, depending on the current density for oxygen production. The profiles become less steep further from the electrode tip or from the bubble and the partial pressure reaches its bulk value at $x = 0.8$–1.2 mm. Fluorescence concentration profiles near oxygen bubbles or other interfaces exhibit similar shapes and the profiles for oxygen should be corrected for the presence of the other phase.

It has been shown that in spite of the inevitable side signal involved in the measurement technique, oxygen supersaturation can be observed by fluorescence quenching:

(i) for current densities greater than 100 A m^{-2}, the signal induced by the presence of the bubble is of a lesser importance compared to that due to actual oxygen supersaturation;

(ii) The technique can be used to measure the oxygen supersaturation in a zone of appreciable thickness from the electrode surface. For the case treated here of a stationary fluid, this thickness is in the range 0.6–1.2 mm, which is far larger than the layer thickness reported in [12]. Supersaturation phenomena are related to electrode processes and mass transfer through the gas–liquid interface. Therefore, the order of magnitude for the thickness of the supersaturation zone surrounding the bubble, corresponds to that of the diffusion layer in almost stagnant flow. In real electrolytic cells, where higher turbulence is ensured by bubble detachment from the electrode surface, it is to be expected that supersaturation in oxygen production will be observed over a much thinner layer.

6. Conclusion

This paper presents the first results of the use of a photophysical technique for the measurement of local concentrations of a dissolved compound. The technique has been used to determine oxygen concentration profiles and demonstrates the phenomenon of supersaturation of an electrogenerated species. Side-reflection and diffraction of both the incident laser beam and the emitted fluorescence at the bubble interface change the signal in a significant manner, especially close to the electrode. Nevertheless, the profiles obtained further from the electrode tip are quite reliable. Further work will report measurements of profiles at the top of the electrode and a more accurate interpretation of the results.

References

[1] D. Bonvallot, J. C. André, E. Français and G. Valentin, *in* 'Récents Progrès en Génie des Procédés', Lavoisier, Paris, **16**, (1991) p. 211.
[2] J. P. Glas and J. W. Westwater, *Int. J. Heat Mass Transfer* **7** (1984) 1427.
[3] H. Vogt, *Electrochim. Acta* **34**(10), (1989) 1429. See also *ibid.* **29**(2), (1984) 167 and 175.
[4] S. Shibata, *Bull. Chem. Soc. Japan* **33**(12), (1960) 1935.
[5] *Idem*, *ibid.* **36**(1), (1963) 53.
[6] C. K. Bon and C. W. Tobias, *J. Electrochem. Soc.* **115**(3), (1968) 91C.
[7] S. Shibata, *Electrochim. Acta* **23** (1978) 619.
[8] L. J. J. Janssen and B. Barendrecht, *ibid.* **29**(9), (1984) 1207.
[9] E. A. Khomskaya and A. S. Kolosov, *Elektrokhimiya* **6**(2), (1970) 256.
[10] E. A. Khomskaya, A. S. Kolosov, Yu. M. Ol'khovnikov and V. I. Eidman, *ibid.* **7**(6), (1971) 876.
[11] E. A. Khomskaya, A. S. Kolosov and V. V. Polishchuk, *ibid.* **7**(7), (1971) 1064.
[12] V. G. Nefedov, V. M. Serebrit-skii, V. V. Matveev and O. S. Ksenzhek, *ibid.* **27**(12), (1991) 1625.
[13] E. Köhler, *Appl. Fluorescence Technology*, **1**, Apr. (1989) 13.
[14] L. J. J. Janssen and J. H. Hoogland, *Electrochim. Acta* **15** (1970) 1013.